Engineering Fracture Mechanics 195 (2018) 297–312

Contents lists available at ScienceDirect

Engineering Fracture Mechanics

journal homepage: www.elsevier.com/locate/engfracmech

Fracture toughness testing using non-standard bend specimens – Part II: Experiments and evaluation of T_0 reference temperature for a low alloy structural steel

Vitor S. Barbosa, Claudio Ruggieri*

Department of Naval Architecture and Ocean Engineering, University of São Paulo, São Paulo, Brazil

ARTICLE INFO

Keywords:
Fracture toughness test
J-integral
Specimen geometry effect
Loading mode effect
Subsize specimen
Reference temperature

ABSTRACT

The present study addresses an experimental investigation of the effects of geometry and loading mode on the cleavage fracture behavior of a high strength, low alloy structural steel using standard and non-standard SE(B) specimens, including a non-standard PCVN configuration. Fracture toughness testing conducted on various bend specimen geometries extracted from an A572 Grade 50 steel plate provides the cleavage fracture resistance data in terms of the *J*-integral at cleavage instability, J_c. The experimental results show a potential effect of specimen geometry and loading mode on J_c-values which can help mitigating the effects of constraint loss often observed in smaller fracture specimens. An exploratory application to determine the reference temperature, T_0, derived from the Master Curve methodology (which defines the dependence of fracture toughness with temperature for the tested material) also provides additional support for using non-standard bend specimens in routine fracture applications.

1. Introduction

Accurate assessments of fracture behavior remain essential in design, fabrication and fitness-for-service (FFS) methodologies (often typified by, for example, repair decisions and life-extension programs) while, at the same time, ensuring acceptable safety levels during normal operation for a wide class of engineering structures, including pressure vessels, piping systems and a variety of other structural applications such as heavy construction equipment and heavy duty anchoring systems, among others. For ferritic materials, such as carbon and low-alloy steels typically used in structural components, at temperatures in the ductile-to-brittle transition (DBT) region, unstable fracture by transgranular cleavage represents one of the most serious failure modes as local crack-tip instability may trigger catastrophic structural failure at low applied stresses with little plastic deformation. This type of structural failure almost invariably initiates at crack-like defects formed during in-service operation most often resulting from planar flaws in weldments (*e.g.*, hot or cold cracking, lack of penetration, undercut) [1,2], fatigue cracks, environmentally assisted embrittlement, among others. Several engineering codes and standards thus require minimum levels of fracture toughness at specified temperatures for these materials such that the structure remains safe under normal operation conditions or, perhaps more importantly, during an emergency, equipment failure or an unplanned maintenance event.

Current engineering procedures to quantify service-induced material toughness degradation in ferritic structural steels strongly rely on assessing the shift in the ductile to brittle transition (DBT) temperature in which the measured transition temperature increases with increased toughness degradation. Early procedures adopted a Charpy V-notch (CVN) index temperature shift at 41 J as

* Corresponding author.
E-mail address: claudio.ruggieri@usp.br (C. Ruggieri).

https://doi.org/10.1016/j.engfracmech.2018.03.028
Received 6 January 2018; Received in revised form 22 March 2018; Accepted 26 March 2018
Available online 05 April 2018
0013-7944/

a toughness degradation criterion but recent developments based on fracture mechanics concepts led to a more rational approach, often known as the Master Curve approach [3–6] and standardized in the form of ASTM E1921 [7], to define an indexing (or reference) temperature, T_0, related to the median fracture toughness of K_{Jc}-values experimentally measured from standard 1T fracture specimens; here, the fracture toughness characterized in terms of K_J is determined using the standard relationship $J = (1-\nu^2)K_J^2/E$ where E is the elastic longitudinal modulus and ν is Poisson's ratio. Previous studies [8,9,5] have shown that the Master Curve methodology is highly effective in describing the dependence of fracture toughness on temperature for a wide range of pressure vessel steels, irradiated steels and other structural ferritic steels.

Despite representing a significant advance in fracture testing programs to characterize material toughness degradation, one key issue to resolve with the Master Curve methodology concerns the sensitivity of T_0 on specimen size, particularly when subsize configurations are employed to measure the fracture toughness properties. One application of considerable interest involves structural integrity assessments of commercial reactor pressure vessels (RPVs) and the associated primary pressure boundary system. In routine RPV surveillance programs to measure the transition temperature shift, three-point bend testing of precracked Charpy-type (PCVN) specimens (which were included in capsules located on the inside of the RPV and exposed to high-energy neutrons [10]) becomes necessary in macroscopic measurements of cleavage fracture toughness (such as the J-integral at cleavage instability, J_c, or the corresponding K_{Jc}-value) due to severe limitations on material availability. Similarly, a number of recent applications also involve the use of small-scale fracture specimens to measure fracture toughness properties when limited material availability and test machine capacity are of major concern. These applications include, for example, fracture toughness measurements of specific microstructures in the heat affected zone of girth welds for relatively thin-walled pipelines.

However, as the specimen size is reduced (relative to the standard 1T specimen), the evolving crack-tip plastic zones developing from the free surfaces with increased loading affect strongly the crack front size over which high levels of near-tip stress triaxiality (constraint) are maintained. These changes in the crack-tip stress fields over a relatively small thickness in connection with a smaller sampling volume for cleavage fracture influence the measured toughness values, including their statistical scatter and average value (either the mean and the median values). Such features clearly affect the fracture toughness dependence on temperature and, consequently, produce potential differences in T_0-values measured using small size specimens and larger fracture specimens. Indeed, previous test programs have identified differences in T_0-values estimated from PCVN specimens spanning a relatively wide range of temperatures (typically from a few degrees to as much as 40–45 °C), when compared to T_0-values measured using larger specimens [11]. An illustrative example includes fracture toughness results from the Heavy-Section Steel Irradiation (HSSI) Program conducted at Oak Ridge National Laboratory (ORNL) [12] from which the reference temperature, T_0, was evaluated for the beltline weld of a typical pressurized water reactor (PWR) using toughness results measured from standard 1T C(T) specimens and PCVN geometries. As reported in [11], the T_0 evaluated from the PCVN specimens is 21 °C lower than the corresponding value measured using the 1T C(T) configuration.

In Part I of this article [13], a fracture toughness test procedure applicable to bend geometries with varying specimen span over width ratio (a/W) and loaded under 3-point and 4-point bend loading was presented. In particular, a new set of plastic η-factors applicable to fracture testing of non-standard bend geometries was provided. The present study builds upon that work to address an experimental investigation of the effects of geometry and loading mode on the cleavage fracture behavior of a high strength, low alloy structural steel using standard and non-standard SE(B) specimens, including a non-standard PCVN configuration. Fracture toughness testing conducted on various bend specimen geometries extracted from an A572 Grade 50 steel plate provides the cleavage fracture resistance data in terms of the J-integral at cleavage instability, J_c. The experimental results show a potential effect of specimen geometry and loading mode on J_c-values which can help mitigating the effects of constraint loss often observed in smaller fracture specimens. An exploratory application to determine the reference temperature, T_0, derived from the Master Curve methodology (which defines the dependence of fracture toughness with temperature for the tested material) also provides additional support for using non-standard bend specimens in routine fracture applications.

2. Experimental program

2.1. Material description and mechanical properties

The material utilized in this study is a typical ASTM A572 Grade 50 structural steel with 376 MPa yield stress and 555 MPa tensile strength at room temperature (20°) supplied as a hot rolled plate with a nominal thickness of 31.5 mm. Table 1 lists the chemical composition for the tested material which contains less amount of C than the maximum value specified in ASTM A572 standard [14]. The required mechanical strength is then obtained by small additions of key microalloying elements, such as Nb, V and Ti, as shown in Table 1. Metallographic examination of an etched surface of the tested steel displayed in Fig. 1 revealed a layered microstructure aligned with the plate rolling direction, with refined grains of ferrite and colonies of pearlite.

Mechanical tensile tests conducted on standard tensile specimens with 12.5 mm diameter extracted from the transverse plate

Table 1
Chemical composition of tested ASTM A572 Grade 50 (% weight).

C	Mn	Nb	V	Ti	Cr	Ni	Mo
0.15	1.46	0.037	0.005	0.031	0.02	0.02	0.01

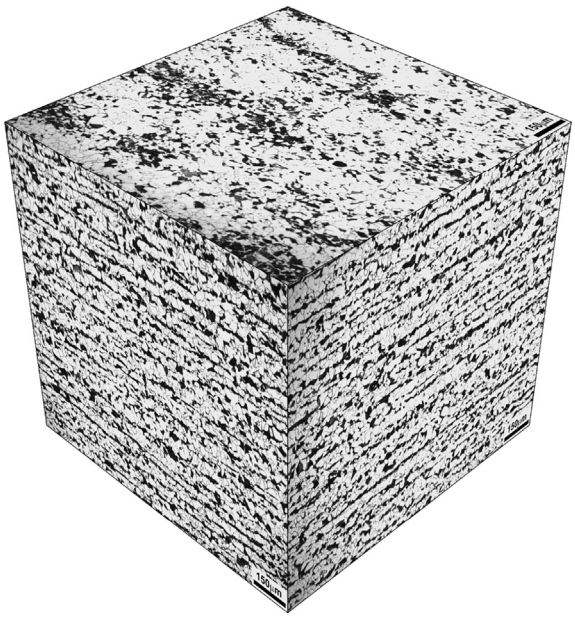

Fig. 1. 3D view of the microstructure for the tested ASTM A572 Gr 50 steel (Etching: Nital 2%. Magnification: 100×).

direction provide the room temperature ($T = 20$ °C) stress–strain data. These test pieces were loaded in a 250 kN MTS servo-hydraulic universal testing machine with an axial extensometer to measure the specimen elongation according to ASTM E8M [15] requirements. Because fracture testing was conducted in the DBT region (see further details next), additional tensile tests were also conducted at $T = -20$ °C on subsize test specimens with 6 mm diameter. Table 2 summarizes the tensile testing results for each test temperature in which the σ_{uts}/σ_{ys}-ratio of 1.5 is in the typical range for this class of normalized steel and evidence a relatively moderate hardening behavior. Other mechanical properties for this material include Young's modulus, $E = 201$ GPa and Poisson's ratio, $\nu = 0.3$. Fig. 2(a) provides the engineering stress-strain curve for the ASTM A572 Grade 50 steel at room temperature and at $T = -20$ °C (average stress-strain response using data from three test specimens). For reference, an improved estimate for the hardening exponent given by Annex F of API 579 [16] provides the strain hardening exponents at the test temperatures (refer to Table 2) as $n = 8$.

A set of 30 Charpy-V notch (CVN) impact specimens was extracted in the T-L plate orientation. This set was tested in a 400 J full-scale Tinius-Olsen pendulum machine following the requirements of ASTM E23 standard [17]. The specimens were tested at 10 different temperatures: −66 °C, −56 °C, −42 °C, −25 °C, −15 °C, 0 °C, 9C, 27 °C, 50 °C and 66 °C. Fig. 2(b) shows the measured toughness-temperature properties for the material in terms of conventional Charpy V-notch impact energy (T-L orientation). In this plot, the symbols represent the experimentally measured Charpy energy and the solid line defines a hyperbolic tangent curve fitting proposed by Kirk et al. [18] in the form

$$CVE = 56 + 50\tanh\left[\frac{T+5}{27}\right] \quad \text{°C, J} \tag{1}$$

where CVE denotes the Charpy V-notch energy expressed in J and T is the test temperature in degrees Celsius. Using the above expression, the Charpy transition temperatures corresponding to 28 J and 41 J energy yield approximately $T_{CVN}^{28J} = -22$ °C and $T_{CVN}^{41J} = -13$ °C.

2.2. Fracture toughness testing

Fracture toughness tests were performed on conventional, plane-sided three-point bend fracture specimens with varying crack sizes and specimen thickness in the T-L orientation as illustrated in Fig. 3. Testing of these configurations was performed at $T = -20$ °C; as shown previously in Fig. 2(b), this temperature corresponds to the lower-shelf, ductile-to-brittle transition behavior

Table 2
Tensile properties of tested A572 Gr 50 steel at different test temperatures measured from transverse plate direction at mid-thickness location (σ_{ys} and σ_{uts} denote the yield stress and tensile strength while ϵ_t represents the uniform elongation as per ASTM E8M [15]).

T (°C)	σ_{ys} (MPa)	σ_{uts} (MPa)	σ_{uts}/σ_{ys}	n	ε_t (%)
20	376	555	1.5	8.0	14.2
−20	407	601	1.5	8.0	15.4

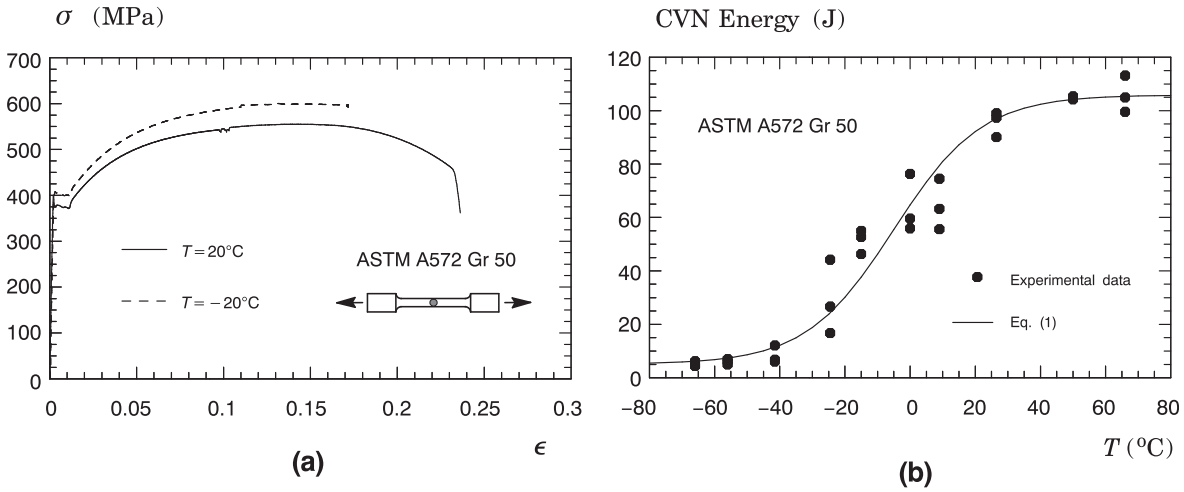

Fig. 2. (a) Engineering stress-strain curve (average stress-strain response using data from three test specimens) for the tested ASTM A572 Grade 50 steel at room temperature and at −20 °C. (b) Charpy-V impact energy (T-L orientation) versus temperature for the tested A572 Gr 50 steel.

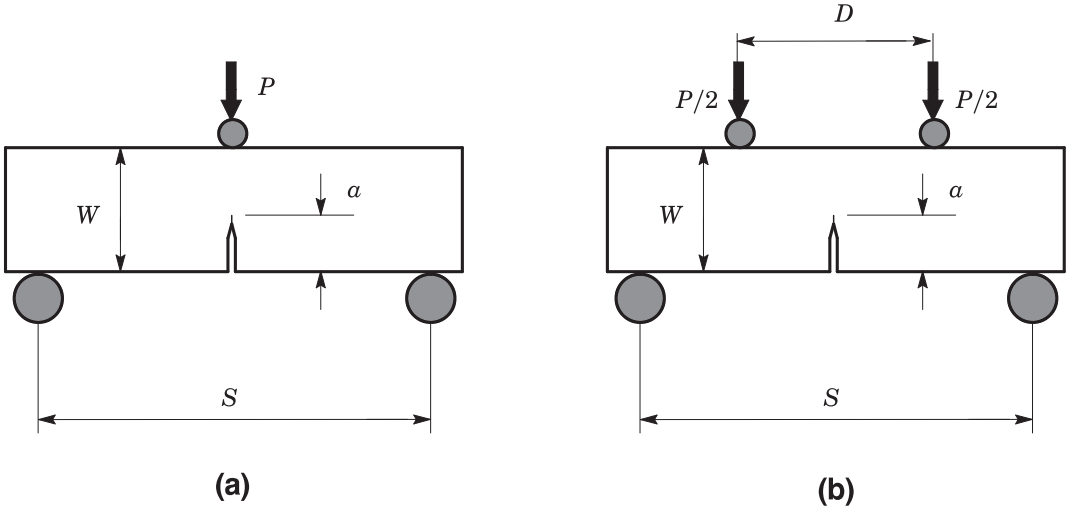

Fig. 3. Bend loading geometries utilized in the fracture tests: (a) 3-point SE(B) specimen. (b) 4-point bend specimen.

for the tested steel. The fracture mechanics tests include: (1) conventional, plane-sided 1T SE(B) specimens with $a/W = 0.5$ and $a/W = 0.2$, $B = 25$ mm, $W = 50$ mm and $S = 4W$ loaded under 3-point bending; (2) plane-sided 0.8T SE(B) specimens with $a/W = 0.5$, $B = 20$ mm, $W = 40$ mm and $6W$ loaded under 3-point and 4-point bending; and (3) plane-sided, precracked Charpy (PCVN) specimen with $a/W = 0.5$, $B = 10$ mm, $W = 10$ mm and $S = 4W$, $6W$ and $8W$ loaded under 3-point bending. Here, a is the crack size, W denotes the specimen width, B represents the specimen thickness and S is the load span. To investigate the potential influence of side groove on the fracture toughness values, fracture tests were also conducted on side-grooved PCVN specimens with $S = 6W$ having a net thickness of 80% the overall thickness (10% side-groove on each side). ASTM E1820 [19] provides additional details for the geometry and dimensions of the tested fracture specimens.

Following the requirements of ASTM E1820 [19] and ASTM E1921 [7], a fatigue precrack was introduced at the machined notch root by cyclic loading all fracture specimens under three-point bending at room temperature. Special care was exercised during the fatigue precracking of the PCVN geometries to ensure that the values of the stress intensity factor attained during the procedure and the amount of fatigue crack growth were fully in accordance with the requirements of ASTM E1921 [7]. The test specimens were immersed in a nitrogen/alcohol bath with temperature controlled by a thermocouple wired to a digital thermometer. The cooling bath temperature was then maintained during 20–30 minutes at the specified test temperature before the test specimens were loaded. Post-test examinations established the amount of fatigue crack growth to determine the initial crack size by adopting a 5-point measurement technique; the technique is very similar to the procedure described in ASTM E1820 [19], but with points along the crack front near the specimen surfaces omitted in the averaging process to avoid including points that exhibit almost no crack extension. A similar technique was employed to measure the amount of ductile tearing, if any, prior to final fracture by cleavage in the tested specimens. Load vs. crack mouth opening displacements (CMOD) records for each specimen were measured using a clip

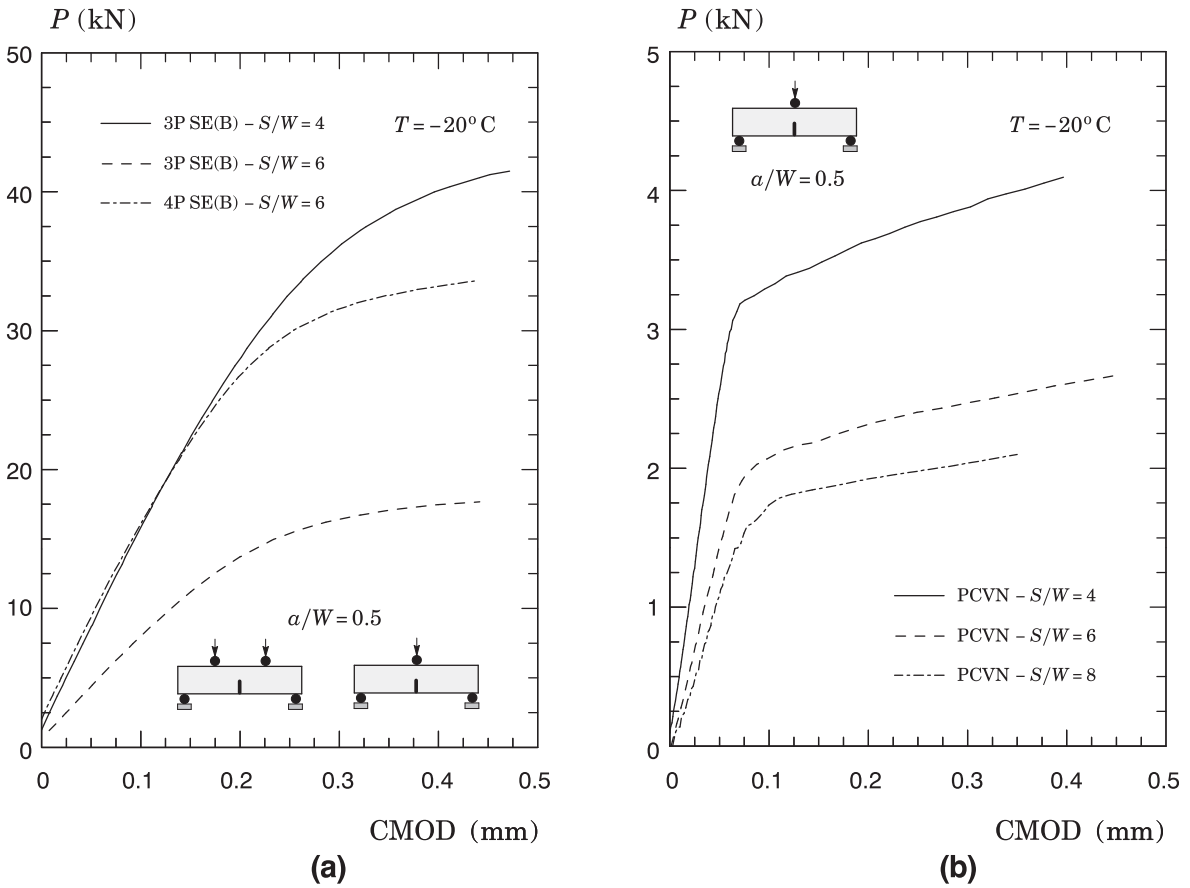

Fig. 4. Representative load-displacement response for the tested geometries with varying specimen span: (a) 3-point and 4-point SE(B) specimens with $a/W = 0.5$. (b) PCVN configurations.

gauge mounted on an integrated knife-edge machined into the notch mouth.

To illustrate the effect of loading mode and specimen span on the load carrying capacity of the tested bend configurations, Fig. 4 shows typical load-displacement curves (as described by CMOD) measured from testing the deeply-cracked SE(B) specimens and the PCVN geometries. In these plots, each of these curves corresponds to a specimen for which the measured J-value is similar to the characteristic toughness, J_0, of the corresponding statistical distribution of measured J_c-values – see Section 3 next. The strong effect of span size associated with specimen geometry is evident in these plots. At similar levels of crack mouth opening displacement, the applied load for the bend specimens with increased span is reduced by approximately a factor of 2 compared to the load response for the standard bend specimen with $S/W = 4$. Moreover, note that the loading mode appears to play a lesser role on the load carrying capacity for the 4P bend geometry with $S/W = 6$ as its load-displacement curve does not differ significantly from the corresponding curve for the standard 1T SE(B) specimen.

Evaluation of cleavage fracture toughness values, here characterized in terms of the J-integral at cleavage instability, J_c, follows from determining the plastic area under the experimentally measured load-CMOD curve and then using the estimation procedure outlined in ASTM E1820 [19]. To determine the J_c-values for the tested bend geometries, including the 4P bend configuration, we employ the η-solutions developed in Part I of the study [13], which are derived from extensive plane-strain analyses conducted on 3P and 4P bend specimens with varying crack sizes and different hardening materials. Tables 3,4 show the fracture toughness at cleavage instability for the ASTM A572 Grade 50 steel obtained from fracture specimens with varying specimen geometries tested at $T = -20$ °C. The tables also include the average precrack fatigue length based on the 5-point measurement technique described earlier. Observe that the measured J_c-values for all tested deeply-cracked SE(B) specimens displayed in Table 3 far exceed the deformation limit, $M = 30$, specified by ASTM E1921 [7]. In contrast, Table 4 clearly shows the reduced measuring capacity of the PCVN configurations as their corresponding M-values at fracture are significantly lower than the corresponding deformation limit values for the deeply-cracked SE(B) specimens and, further, most of the toughness data are closer to the $M = 30$ value. Indeed, several of the toughness values for the PCVN geometries with $S/W = 4$ and 6 exhibit deformation limits at fracture lower than the specified value by ASTM E1921 [7] and are thereby marked as censored data in the procedure to estimate the reference temperature, T_0. These issues will be taken up in the next sections.

Table 3
Measured cleavage fracture toughness values, described in terms of J_c, for the A 572 Gr 50 steel obtained from 3P and 4P SE(B) specimens with varying geometries tested at $T = -20$ °C.

Specimen configuration	Specimen number	J_c [kJ/m^2]	K_{Jc} [MPa m$^{1/2}$]	a_0 [mm]	$M = (b_0\sigma_{ys}/J_c)$
1T 3P SE(B)	16	27	78	25.3	382
$a/W = 0.5$	17	65	121	25.6	159
$S/W = 4$	18	80	135	25.5	128
	19	77	132	25.4	135
	20	43	98	25.6	240
	21	63	119	25.8	162
	22	46	102	25.6	223
	23	65	122	25.3	158
	24	47	103	25.3	222
1T 3P SE(B)	1	81	135	10.1	205
$a/W = 0.2$	2	78	133	10.2	211
$S/W = 4$	3	71	127	10.2	232
	4	84	138	10.3	196
	5	64	120	10.3	259
	6	89	141	10.0	188
	7	89	142	10.1	186
	8	108	156	10.3	153
	9	62	118	10.0	268
0.8T 3P SE(B)	1	58	114	20.3	139
$a/W = 0.5$	2	55	111	20.2	147
$S/W = 6$	3	60	116	20.2	135
	4	32	85	20.1	254
	5	24	74	20.1	336
	6	39	94	20.1	207
	7	81	136	20.2	99
	8	44	99	20.2	184
	9	55	112	20.2	146
0.8T 4P SE(B)	10	68	124	20.1	119
$a/W = 0.5$	11	32	86	20.1	250
$S/W = 6$	12	48	105	19.9	169
	13	61	118	20.0	133
	14	40	95	21.2	193
	15	42	97	20.1	195
	16	68	124	20.3	118
	17	79	133	20.2	102
	18	58	114	20.2	139

3. Effects of specimen geometry and loading mode on J_c-values

Before discussing the effects of specimen geometry and loading on the J_c-distributions, it is helpful to briefly examine some important features of cleavage fracture which have a bearing on the results provided later. Post-mortem examination of the fracture surfaces for all tested SE(B) specimens and PCVN configurations revealed essentially no ductile tearing prior to cleavage fracture thereby providing strong support to the master curve analysis for the tested material described next. Fig. 5(a) displays a typical fracture surface for the deeply-cracked 1T specimen with $a/W = 0.5$ at −20 °C showing no evidence of plastic deformation at the crack front and clear characteristics of brittle fracture. Fig. 5(b) and (c) shows a scanning electron microscopy (SEM) for this fracture surface examined very close to the crack tip region. Observe the relatively well-defined transition between the tip of the fatigue precrack and the beginning of the fracture surface shown in Fig. 5(b) for a relatively lower magnification while Fig. 5(c) clearly reveals well-defined cleavage planes characteristic of stress-controlled cleavage fracture at the same crack tip region under a much larger magnification. Similar features are also observed for the PCVN geometry with $S/W = 6$ as displayed in Fig. 6(a) and (b). Note, however, the relatively larger amount of plasticity that developed in the specimen as revealed by its lateral contraction associated with out-of-plane constraint loss. Also, observe the occurrence a single, albeit relatively small, transverse delamination which further contributes to the increase in measured fracture toughness values. While we have not investigated the precise cause for the development of this delamination crack, we argue that the formation of such transverse crack is primarily associated with the anisotropic microstructural features of the material which govern the separation of transverse weak planes, most likely due to the decohesion of the ferrite-pearlite interface that may occur in layered microstructures (refer to Fig. 1). Similar features are also observed for other tested specimen geometries and are not shown here in interest of space.

Figs. 7 and 8 show the (rank-ordered) cumulative probability distribution of the measured toughness values, J_c, for all tested fracture geometries. The solid and open symbols in the plots indicate the experimental fracture toughness data for the specimens – observe that the open symbols in Fig. 8 represent the J_c-values for the PCVN configurations which exceeded the limit toughness value

Table 4
Measured cleavage fracture toughness values, described in terms of J_c, for the A 572 Gr 50 steel obtained from PCVN geometries with varying specimen span tested at $T = -20$ °C.

Specimen configuration	Specimen number	J_c [kJ/m^2]	K_{Jc} [MPa m$^{1/2}$]	a_0 [mm]	$M = (b_0\sigma_{ys}/J_c)$
PCVN	1	63	119	5.2	31
$S/W = 4$	2	100	150	5.0	20
	3	51	108	5.2	38
	4	54	110	4.9	38
	5	63	120	4.9	33
	6	93	145	5.1	22
	19	78	133	5.1	25
	20	65	121	5.2	30
	21	67	123	5.1	30
	22	97	148	5.2	20
	23	40	96	5.5	46
	24	107	156	5.1	19
	28	60	117	5.2	33
	29	65	121	5.0	31
PCVN	7	75	130	5.2	26
$S/W = 6$	8	103	152	5.1	20
	9	60	116	4.9	35
	10	46	102	4.9	45
	11	59	115	5.1	34
	12	86	140	5.1	23
	13	79	133	5.1	25
	14	92	144	5.2	21
	15	44	100	5.1	45
	16	68	124	4.9	31
	17	37	91	5.1	54
	18	108	156	5.0	19
	25	60	116	4.9	35
	26	81	135	5.0	25
	27	92	144	5.0	22
SG PCVN	42	49	105	4.9	42
$S/W = 6$	43	41	97	5.0	50
	44	41	96	4.9	51
	45	71	127	5.0	28
	46	50	107	5.0	41
	47	62	119	4.9	33
	48	59	116	4.9	35
	49	29	81	4.6	77
	50	45	101	5.0	45
	51	51	108	4.9	40
	52	77	132	5.0	26
	53	47	103	4.7	46
PCVN	30	47	103	5.2	42
$S/W = 8$	31	48	104	5.1	42
	32	80	135	5.0	26
	33	53	110	5.2	37
	34	54	111	4.7	40
	35	38	93	5.0	53
	36	68	123	5.0	30
	37	57	114	5.1	35
	38	57	113	5.0	36
	39	84	138	4.7	26
	40	40	95	5.1	50
	41	53	109	4.9	39

defined by $J_{lim} = (b\sigma_{ys})/M$, with the deformation limit, M, assigned a value of 30 as per ASTM E1921 [7] – see also Table 4. Values of the cumulative failure probability, $F(J_c)$, are obtained by ordering the J_c-values and using $F(J_{c,k}) = (k-0.3)/(N + 0.4)$ [20], where k denotes the rank number and N defines the total number of experimental toughness values. The curves displayed in these plots describe the three-parameter Weibull distribution for J_c-values given by

$$F(J_c) = 1-\exp\left[-\left(\frac{J_c-J_{\min}}{J_0-J_{\min}}\right)^{\alpha}\right] \tag{2}$$

in which α defines the Weibull modulus (which characterizes the scatter in test data), J_0 is the characteristic toughness (which

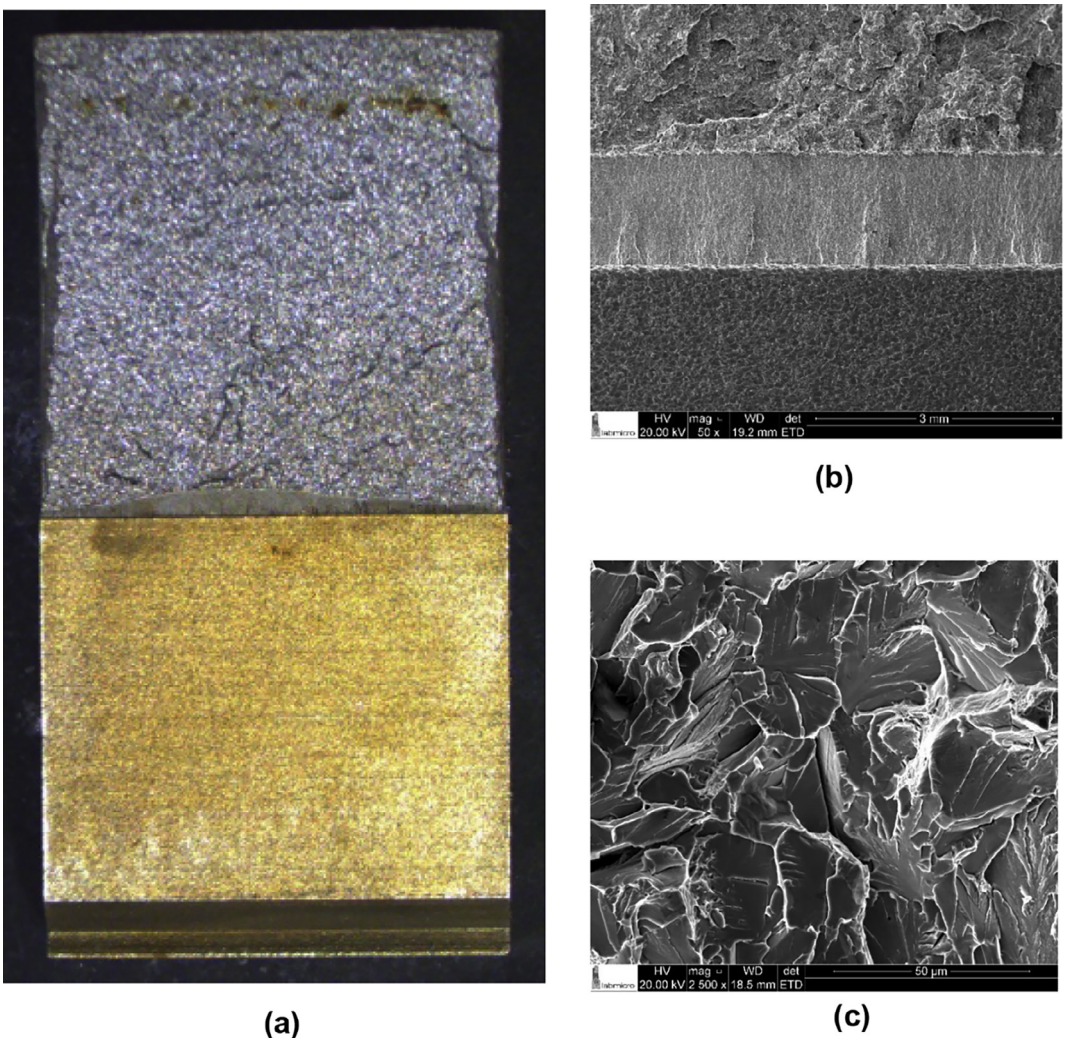

Fig. 5. (a) Typical fracture surface for the 1T SE(B) specimen with $a/W = 0.5$ at $T = -20$ °C showing no evidence of plastic deformation at the crack front; (b) and (c) Scanning electron microscopy (SEM) of the fracture surface.

approximately describes the mean value, J_{mean}, of the test data given by $J_{mean} = J_0\Gamma(1 + \alpha^{-1})$ with Γ defining the Gamma function [20]) and $J_{\min}$ denotes the threshold J-value corresponding to a $K_{\min}$ of 20 MPa$\sqrt{\text{m}}$ as given by ASTM E1921 [7]. Following ASTM E1921 [7] and standard statistical procedures [20], a maximum likelihood (ML) analysis of the data set shown in Figs. 7 and 8 is conducted by adopting a fixed value $\alpha = 2$ for the Weibull modulus of the Weibull distribution for J_c-values with the characteristic toughness, J_0, remaining to be determined. Here, the $\alpha = 2$ is adopted by ASTM E1921 [7] to describe the scatter in test data based on the assumption that the measured J_c-values satisfy parametric limits on the crack-tip deformation relative to crack length, specimen thickness and remaining crack ligament such that high constraint conditions, similar to those of small-scale yielding (SSY), are maintained over microstructurally significant size scales at the crack-tip region. Table 5 provides the ML estimates of the characteristic toughness, J_0, for all tested crack configurations, including the estimated values considering the raw data (without censoring) and considering the censoring model described in ASTM E1921 [7] (see also Mann et al. [20])– these values are denoted as $\hat{J}_{0-NC}$ and $\hat{J}_{0-C}$ in Table 5.

Consider first the experimental toughness distribution for the SE(B) specimens displayed in Fig. 7. Apart from a somewhat different scatter with respect to the theoretical Weibull distribution described by Eq. (2), the experimental results are rather conclusive – the three-point bend geometry with increased specimen span of $S/W = 6$ and $B = 20$ mm (0.8T) provides the lower mean toughness as its J_c-distribution is shifted to the left in comparison to the J_c-distribution for the standard 1T SE(B) specimen. Observe that the toughness distribution for the four-point bend configuration, which also has $B = 20$ mm, is also slightly shifted to the left, albeit similar to the corresponding toughness distribution for the standard SE(B) geometry with $a/W = 0.5$. Note that, despite the somewhat reduced thickness of these non-standard bend geometries, their toughness distributions yield lower mean toughness compared to the standard 1T specimen, which only further emphasizes the role of increased span and loading mode on fracture behavior of bend geometries. Also observe the relatively strong effect of crack size on the measured toughness distribution as the

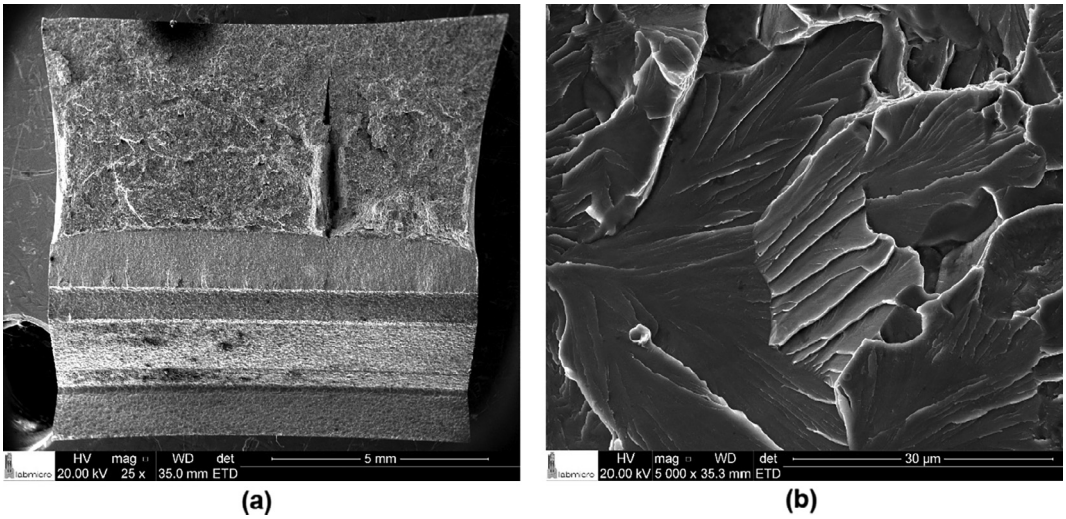

Fig. 6. (a) Typical fracture surface for the PCVN specimen with $S/W = 6$ at $T = -20$ °C. (b) Scanning electron microscopy (SEM) of the fracture surface.

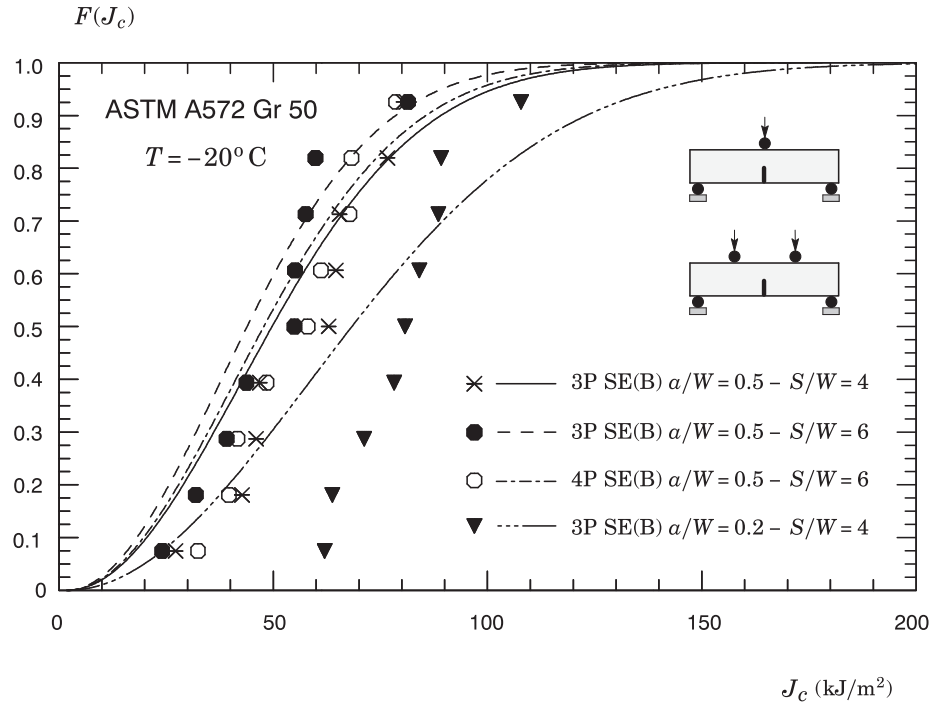

Fig. 7. Cumulative Weibull distribution of experimentally measured J_c-values of the A572 Gr 50 steel for all tested SE(B) fracture specimens.

shallow crack bend specimen with $a/W = 0.2$ provides much larger J_c-values (note here that the scatter for the toughness values corresponding to this specimen geometry deviates rather significantly from the theoretical Weibull distribution described by Eq. (2) with $\alpha = 2$).

Consider next the distribution of J_c-values obtained from the PCVN configurations with varying S/W-ratios shown in Fig. 8. The toughness distribution for the standard SE(B) geometry with $a/W = 0.5$ is also provided on this figure to aid in assessing the relative change in fracture toughness. The trends are clear as the S/W-ratio affects strongly the fracture behavior for this specimen geometry. First, focus attention on the J_c-distribution for the plane-sided PCVN specimen with $S/W = 4$ and $S/W = 6$. Here, the toughness distribution is shifted to the right in comparison to the toughness distribution for the standard 1T SE(B) specimen thereby providing higher mean toughness values. Moreover, a rather significant number of toughness values exceeding the limit toughness, J_{lim}, also occur which poses some difficulties in obtaining reliable estimates of the Weibull distribution parameters [20]. Such behavior can be attributed to the development of plastic deformation coupled with strong constraint loss as the remote loading (as characterized by J

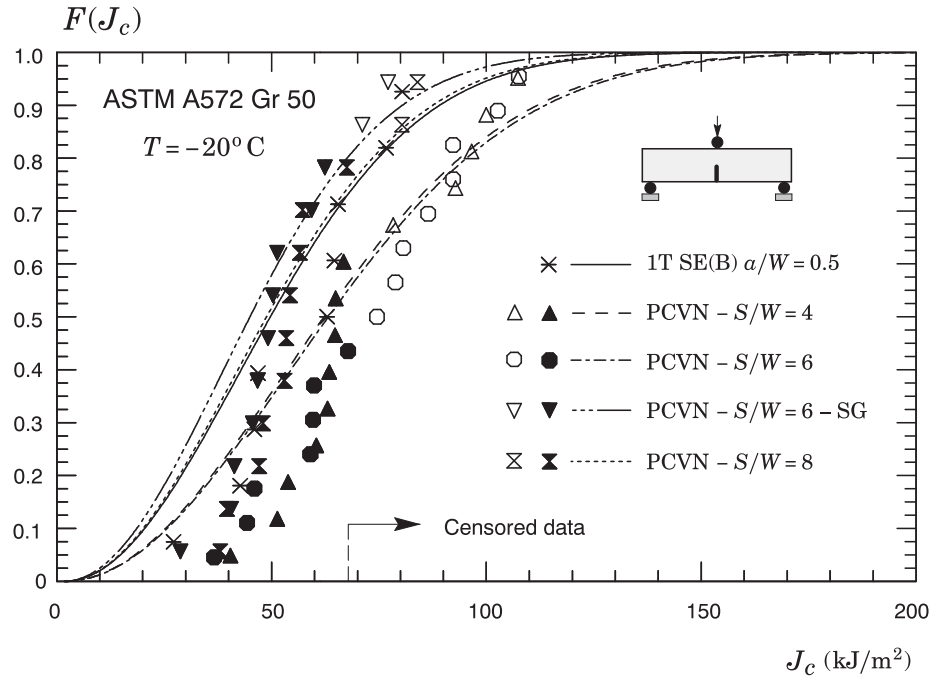

Fig. 8. Cumulative Weibull distribution of experimentally measured J_c-values of the A572 Gr 50 steel for all tested PCVN fracture specimens.

Table 5
Maximum likelihood estimates of the characteristic toughness, $\hat{J}_0$, for the measured distributions of the J_c-values of each specimen geometry and the corresponding estimates for T_0-values.

Geometry	B (mm)	S/W	Loading mode	α	J_{0-NC} (kJ/m^2)	J_{0-C} (kJ/m^2)	T_0 (°C)
SE(B) – $a/W = 0.5$	25	4	3P	2	59	59	−26
SE(B) – $a/W = 0.2$	25	4	3P	2	82	82	n.a
SE(B) – $a/W = 0.5$	20	6	3P	2	52	52	−18
SE(B) – $a/W = 0.5$	20	6	4P	2	57	57	−21
PCVN	10	4	3P	2	74	78	−20
PCVN	10	6	3P	2	76	90	−24
PCVN	10	8	3P	2	58	60	−11
20% SG PCVN	10	6	3P	2	54	57	−9

or K_J in the present context) increases thereby affecting the weakest link mechanism associated with cleavage fracture at the microlevel.

Now examine the J_c-distributions for the side-grooved PCVN specimen with $S/W = 6$ and the plane-sided PCVN geometry with $S/W = 8$. A different picture emerges as both toughness distributions are now shifted to the left and display decreased mean toughness values relative to the standard 1T SE(B) specimen. Also observe that only a reduced number of toughness values exceeding the limit toughness, J_{lim}, occur thereby affecting only slightly the mean value of the corresponding toughness distributions. The implications of this apparent toughness changes for effects of specimen geometry in precracked Charpy (PCVN) configurations on predictions of the reference temperature, T_0, will be addressed next.

4. Evaluation of the reference temperature, T_0

Evaluation of the reference temperature, T_0, described here follows the procedures of ASTM E1921 [7]. To assess the effects of different specimen geometries on T_0, the evaluation procedure employs the fracture toughness distributions measured using all fracture specimen configurations described previously in which the J_c-values at $T = -20$ °C are converted to K_{Jc}-values using the standard relationship [21] expressed by

$$K_{Jc} = \sqrt{\frac{EJ_c}{(1-\nu^2)}}. \tag{3}$$

where it is understood that plane-strain conditions are assumed. Further, the toughness values are required satisfy the maximum K_{Jc} capacity for the specimen, K_{Jc-lim}, given by ASTM E1921 [7] as $K_{Jc-lim} = \sqrt{Eb_0\sigma_{ys}M^{-1}/(1-\nu^2)}$, where b_0 denotes the original crack

ligament size, σ_{ys} is the material yield stress at the test temperature as provided in Table 2 and the deformation limit is set to $M = 30$ as per ASTM E1921 [7]. K_{Jc}-values exceeding the maximum toughness capacity are set to the limiting value and marked for subsequent censoring. Moreover, for fracture tests performed on other than 1T specimens, the measured toughness values are corrected to their 1T equivalent values using a simple weakest link statistics expressed by

$$K_{Jc-1T} = 20 + (K_{Jc-X}-20)\left(\frac{B_X}{B_{1T}}\right)^{1/4} \quad \text{MPa}\sqrt{\text{m}} \tag{4}$$

where B_{1T} is the 1T specimen size (25 mm) and B_X is the corresponding dimension of the test specimens.

The approach determines the reference temperature, T_0, from evaluation of the median toughness at the tested temperature given by

$$K_{Jc-med} = 0.9124(K_0-20) + 20 \quad \text{MPa}\sqrt{\text{m}} \tag{5}$$

in which K_0 is the characteristic toughness of the three-parameter Weibull distribution [20] to describe the distribution of toughness values in the form

$$F(K_{Jc}) = 1-\exp\left[-\left(\frac{K_{Jc}-K_{\min}}{K_0-K_{\min}}\right)^{\alpha}\right] \tag{6}$$

in which the Weibull modulus, α, takes the value of 4, $K_{\min}$ defines a threshold fracture toughness (*i.e.*, $F(K_{Jc}) = 0$ for $K_{Jc} \leqslant K_{\min}$) most often assigned a value of 20 MPa$\sqrt{\text{m}}$. Readers are referred to the work of Wallin [5], McCabe et al. [6] and ASTM E1921 [7] for a more comprehensive description of the Master Curve methodology.

In the present study, evaluation of the reference temperature for the 1T SE(B) specimen with $a/W = 0.5$ is considered first to provide a baseline value for T_0 against which all other values can be compared. Because these fracture specimens have thickness $B = 25$ mm, the K_{Jc}-values for this geometry are taken directly as 1T size toughness values as described in ASTM E1921 [7]. Moreover, all measured K_{Jc}-values at $T = -20$ °C for this specimen are considered valid tests – observe in Table 5 that the M-values for this specimen geometry largely exceed the specified deformation limit of 30. Once a K_0-value for the SE(B) specimen with $a/W = 0.5$ is determined using a maximum likelihood estimation procedure [20], the reference temperature is obtained by simply determining the median toughness, K_{Jc-med}, as defined in previous Eq. (5). The procedure is relatively simple and straightforward while, at the same time, representing well the statistical distribution of measured cleavage fracture toughness data. For the tested structural steel, the reference temperature then yields the value of $T_0 = -26$ °C which is about −6 degrees below the test temperature – this T_0-value is thus considered a "baseline" reference temperature in the present study. Fig. 9 provides the variation of cleavage fracture toughness with temperature for this specimen. In this plot, the solid line defines the master curve of median toughness, K_{Jc-med}, for 1T specimens

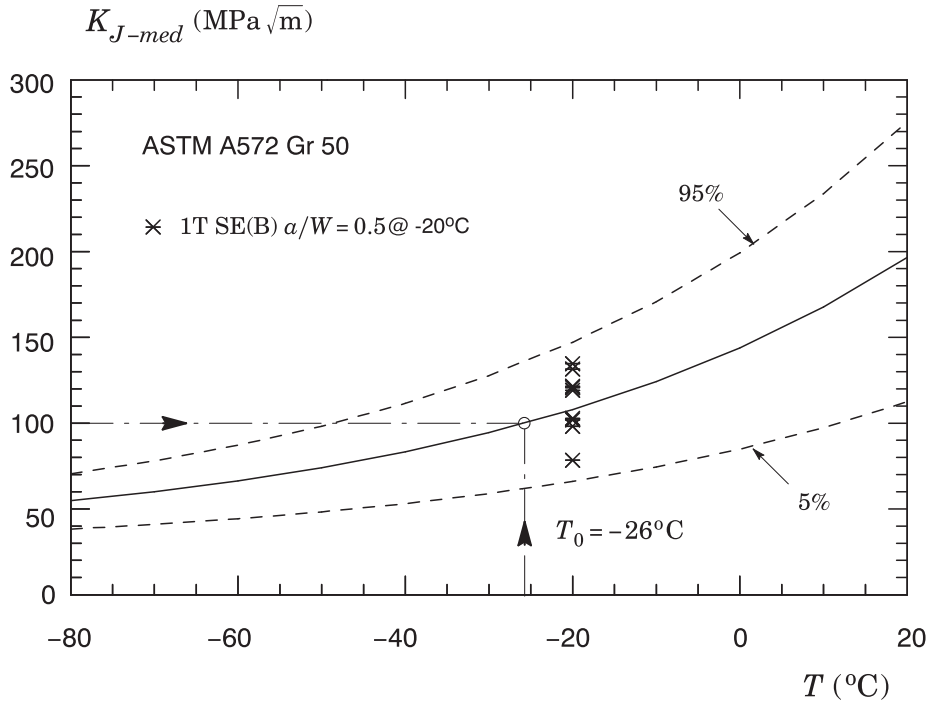

Fig. 9. Master curve for the tested ASTM A572 Gr 50 steel including 5% and 95% confidence bounds based on cleavage fracture toughness values measured from standard 1T SE(B) specimens with $a/W = 0.5$.

given by

$$K_{Jc-med} = 30 + 70\exp[0.019(T + 26)] \quad °C, MPa\sqrt{m}, \tag{7}$$

where T is the test temperature and the dashed lines represent the 5% and 95% confidence bounds for the maximum likelihood estimate of K_0 – refer to the procedures given by ASTM E1921 [7] to construct confidence bounds for the master curve analysis. The valid measured K_{Jc}-values at $T = -20$ °C are included in the plot to aid in assessing the relative position of the master curve and, at the same time, the significance of the confidence bounds in enveloping the fracture toughness data. Since the test temperature of $T = -20$ °C is close to the T_0-value of −26 °C evaluated for the tested material, the master curve defined by Eq. (7) can thus be considered a good description of the variation of cleavage fracture toughness with temperature in the DBT region for the tested ASTM A572 Grade 50 steel. Moreover, a comparison of the results derived from the present master curve analysis with the measured Charpy energy data displayed in Fig. 2(b) reveals only a small difference between the reference temperature ($T_0 = -26$ °C) and the Charpy transition temperature corresponding to a 28 J energy defined by $T_{CVN}^{28J} = -22$ °C.

Once T_0 is determined for the 1T SE(B) specimen as outlined above, the evaluation procedure of the reference temperature for the tested material proceeds using the fracture toughness distributions for other specimen geometries, including the PCVN configurations. As already discussed before, we observe that testing of the PCVN geometries resulted in a number of invalid or censored toughness data points as indicated by the open symbols in Fig. 8. ASTM E1921 [7] also provides guidelines to treat fracture toughness values exceeding K_{Jc-lim} and to determine T_0 in case of censored toughness distributions – see also Mann et al. [20]. Moreover, also observe that the toughness values for the specimen geometries having reduced thickness are corrected to their 1T equivalent values using a simple weakest link statistics also described in ASTM E1921 [7] thereby reducing the (apparent) sensitivity of K_0 (and, consequently, K_{Jc-med}) on specimen geometry. Table 5 compares the T_0-values obtained from the different specimen geometries tested at $T = -20$ °C in which there is a clear and marked effect of specimen geometry and loading mode on the estimates for T_0-values. The non-standard 0.8T SE(B) specimens with $S/W = 6$ provide slightly lower J_0-values compared to the standard 1T SE(B) specimen thereby producing somewhat higher (and more conservative) estimates for T_0-values.

To further illustrate the effect of specimen span on T_0 determined from using subsize specimens, Figs. 10–12 provide the variation of K_{Jc-med} with temperature for selected PCVN configurations, which include: (1) PCVN geometry with $S/W = 4$; (2) Side-grooved PCVN configuration with $S/W = 6$ and (3) PCVN specimen with $S/W = 8$. In these plots, the solid line again defines the master curve of (corrected) median toughness, K_{Jc-med}, for 1T specimens whereas the dashed lines represent the 5% and 95% confidence bounds for the maximum likelihood estimate of K_0. The significant features include: (1) T_0 increases with increased specimen span relative to the reference temperature determined for the PCVN geometry with $S/W = 4$; (2) equipping the specimen with side-groove and increasing the specimen span appear to strongly limit the effects of constraint loss on measured fracture toughness for the PCVN configuration and on T_0; (3) increasing the specimen span in plane-sided specimens to S/W-ratios of ~ 8 is also effective in limiting the influence of constraint loss on measured fracture toughness for the PCVN configuration and on T_0 and (4) increasing the specimen span appears to

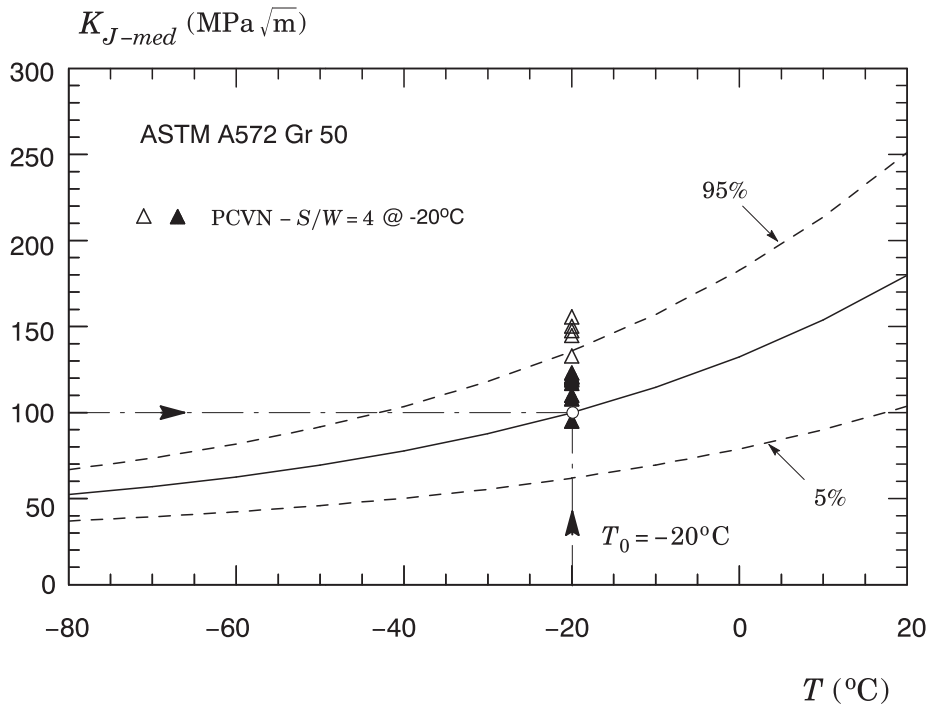

Fig. 10. Master curve for the tested ASTM A572 Gr 50 steel including 5% and 95% confidence bounds based on cleavage fracture toughness values measured from PCVN specimens with $S/W = 4$.

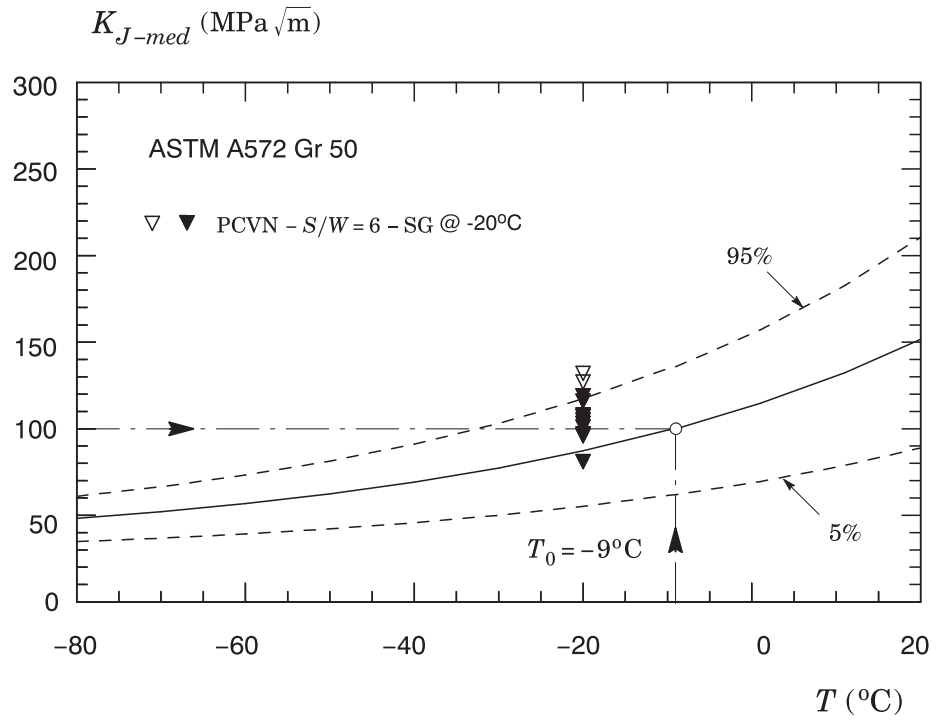

Fig. 11. Master curve for the tested ASTM A572 Gr 50 steel including 5% and 95% confidence bounds based on cleavage fracture toughness values measured from side-grooved PCVN specimens with $S/W = 6$.

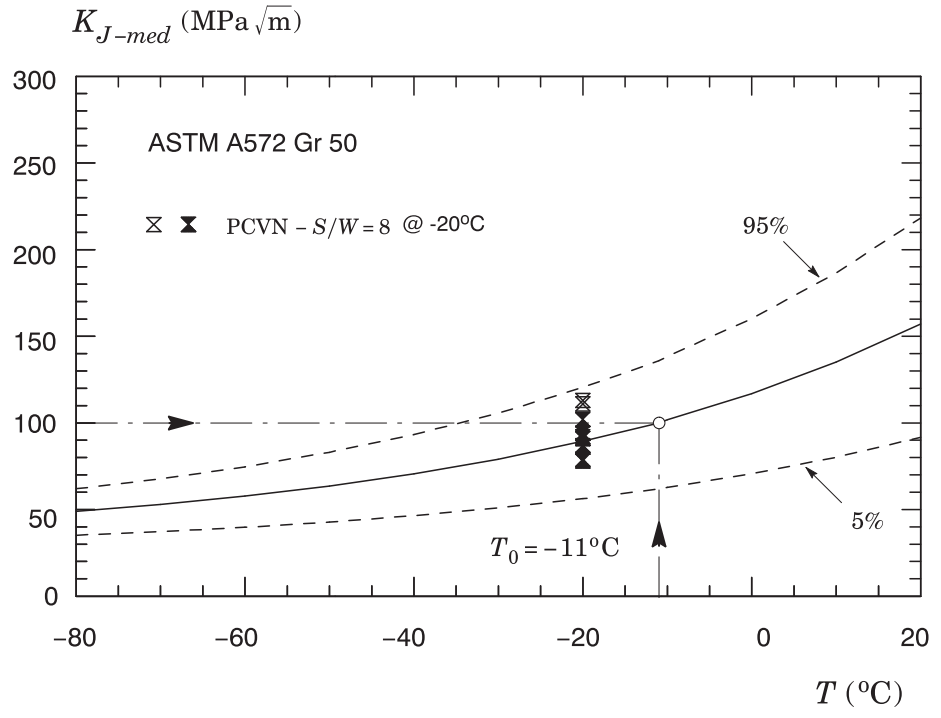

Fig. 12. Master curve for the tested ASTM A572 Gr 50 steel including 5% and 95% confidence bounds based on cleavage fracture toughness values measured from PCVN specimens with $S/W = 8$.

produce a smaller number of invalid (censored) toughness values thereby resulting in more reliable estimates of K_0 and a better statistical description of the measured toughness distribution. Clearly, this latter results are strongly suggestive of the effectiveness of the non-standard PCVN geometry with increased span in mitigating the effects of constraint loss on T_0-estimates often observed in standard PCVN configurations.

5. Discussion and conclusions

This study describes the results of a rather extensive fracture testing of an ASTM A572 Gr 50 structural steel using non-standard bend specimens and an exploratory application to determine the reference temperature, T_0, and associated variation of cleavage fracture toughness with temperature for this material. Fracture toughness tests were conducted on bend configurations with varying specimen geometries and subjected to different bend loading modes. The tests were performed on single edge bend SE(B) specimens in 3-point and 4-point loading with varying crack sizes and specimen thickness covering: (1) standard 1T SE(B) specimens with $a/W = 0.5$ and $a/W = 0.2$, (2) non-standard 0.8T SE(B) specimens with $a/W = 0.5$ and $S/W = 6$ loaded under 3-point and 4-point flexural configuration, and (3) deeply-cracked precracked Charpy notch (PCVN) specimens with $S/W = 4$, 6 and 8. The estimation procedure based on plastic work and load-CMOD records developed in Part I [13] was utilized to evaluate the measured values of J-integral at cleavage instability, J_c, for the tested configurations.

The experimental results clearly show a relatively strong effect of increased specimen span and loading mode on measured J_c-values for the tested material. However, the fracture tests results also suggest that increasing the specimen span to $S/W = 6$ in plane-sided bend geometries appears to have no significant influence on fracture behavior (relative to the standard S/W-ratio of 4). Indeed, only when the specimen span is increased to $S/W = 8$, a more pronounced effect on fracture toughness is noted. Further, equipping the bend specimen having $S/W = 6$ with side-grooves does maintain the measuring capacity of this specimen configuration and helps mitigating the effects of constraint loss often observed in smaller fracture specimens. The experimental results also show that the effects of loading mode on the toughness behavior are relatively small as the measured J_c-distributions for the 3P and 4P bend specimens are similar. To a large extent, these conclusions are supported by our studies performed in Part I [13] in which the levels of crack-tip constraint, characterized in terms of $J-Q$ trajectories, for standard and non-standard bend specimens show a rather marked effect of specimen span and loading mode on fracture behavior for these specimen geometry, particularly for deep crack configurations.

An exploratory application to determine the reference temperature, T_0, based on the Master Curve approach using fracture toughness values obtained from testing non-standard bend geometries, particularly the PCVN configuration with increased span, produces estimates for T_0 which are more conservative than the corresponding reference temperature derived from testing conventional, deeply-cracked 1-T SE(B) specimens. While these results derive directly from the increase in crack-tip constraint with increased specimen span (thereby reducing the characteristic toughness, described in terms of J_0 or K_0, of the measured toughness distribution), they deserve further discussion. Consider first the T_0-estimates derived from the 0.8T bend specimens in comparison with the corresponding estimates for the standard 1T SE(B) specimen shown in previous Table 5. Because of the increased levels of crack-tip constraint here associated with increased span ($S/W = 6$) and 4P loading mode, the reduced K_0-value for these specimen configurations increases T_0 when compared with the baseline reference temperature of −26 °C for the standard 1T SE(B) specimen. Now, compare the T_0-estimates derived from the PCVN geometries with the corresponding estimates for the standard 1T SE(B) specimen shown in previous Table 5. Consider first the PCVN specimen with a standard specimen span of $S/W = 4$. Here, the T_0-estimate is also increased in relation to the baseline T_0 (a difference of 6 °C), a stark contrast to the results reported in [11] in which the T_0 evaluated from PCVN specimens is 21 °C lower than the corresponding value measured using the 1T C(T) configuration (at this point, it must be emphasized the fracture tests reported in [11] were conducted at different temperatures whereas the present study performed all toughness tests at the same temperature of −20 °C). Direct now attention to the 20% side-grooved PCVN specimen with $S/W = 6$ and the plane-sided PCVN geometry with $S/W = 8$. Differences between T_0-estimates for these configurations and the 1T SE(B) specimen are even larger with the T_0 for these specimens yielding −9 °C and −11 °C. Moreover, these latter specimen configurations produce a smaller number of invalid (censored) toughness values thereby resulting in more reliable estimates of T_0 when compared to the corresponding value for the PCVN specimen with $S/W = 4$.

Reading from these results, an argument can be made to plausibly explain the more conservative estimates for T_0 derived from testing PCVN specimens. ASTM E1921 [7] (and other similar procedures as well) adopt simple weakest link arguments to correct K_{Jc}-values for similar fracture specimens with different thicknesses in form of previous Eq. (4). The weakest link assumption thus implies that each point along the crack front for both specimen geometries experiences the same local crack driving force value and the same local stress field. Perhaps more importantly, though, Eq. (4) does not take account the individual contribution of all material points along the crack front into the total failure probability since it attributes equal weight to all of them. Nevalainen and Dodds [22] have addressed this issue to propose an effective thickness, B_{eff}, entering into Eq. (4), rather than the actual specimen thickness, to correct fracture toughness values for thickness effects. As an illustrative example, consider the T_0-estimate derived from the measured J_c-values for the PCVN geometry with the standard specimen span of $S/W = 4$ and the deeply-cracked 1T SE(B) specimen (refer to Table 5, and Figs. 9 and 10). Previous work of Ruggieri et al. [23] shows contour maps of the maximum principal stress, σ_1, for which $\sigma_1 \geqslant 2\sigma_{ys}$ over the crack front for a deeply-cracked SE(B) specimen and a PCVN configuration with $S/W = 4$ in which the size and spatial extent of the distribution of σ_1 over the crack front for the PCVN geometry contrast markedly with those for the deeply-cracked SE(B) specimen. Based on these findings, a rough estimate of B_{eff} for these specimen geometries, which seem approximately compatible with the Ruggieri et al. [23] analyses, is tentatively used here by assuming $B_{eff} = 0.5B$ for the 1T SE(B) specimen and $B_{eff} = 0.75B$ for the PCVN geometry. Based on these new values, we can therefore apply again the Master Curve procedure outline

above thereby now yielding $T_0 = -15°C$ for both specimen configurations. Thus, the concept of B_{eff} appears to alleviate the often observed undercorrection of measured toughness values associated with straightforward application of Eq. (4) in which the actual specimen thickness is used. However, we make no claim about the suitability of such an approach and consider this issue still unresolved with an investigation along this line in progress.

The present study provides additional support for using non-standard bend specimens as an alternative specimen geometry in routine fracture assessments, including the use of small-scale fracture specimens to measure fracture toughness properties when limited material availability is a major concern. A potential application which is gaining increased interest involves fracture toughness measurements of pipeline girth welds of relatively thin-walled pipes, such as carbon dioxide (CO_2) transmission pipelines. Operational and economic factors often dictate the transportation of CO_2 over long distance pipelines as a dense phase, particularly in the supercritical state, due to its low viscosity and high density. However, while cost effective, transporting CO_2 in the dense phase condition significantly increases the risk of brittle failure in the pipeline infrastructure, including operating valves, pumps and compressors, caused by rapid depressurization derived from a pipe leakage (most likely associated with in-service, though-thickness flaws). Because CO_2 undergoes a significant Joule–Thomson cooling effect [24], a sudden decompression of the dense phase into gas leads to very low local temperatures of about −80 °C with a strong potential for unstable cleavage fracture to occur. Because of the relative complexity in conducting standard fracture tests on thin-walled pipeline girth welds, conventional testing programs to measure the fracture toughness of CO_2 pipeline steels in the ductile-to-brittle transition region (DBT) routinely employ the Drop Weight Tear Test (DWTT) and Charpy Notch Impact Test (CVN) to estimate plane-strain fracture toughness values (K_{Ic}) derived from simple correlations between impact energy and fracture toughness [25]. Clearly, as the present investigation shows, the use of small-scale fracture bend specimens with increased span here can be highly effective in producing reliable estimates of cleavage fracture toughness under relatively high levels of near-tip stress triaxiality (constraint). On-going work also investigates the effects of constraint in a 3-D framework on the fracture behavior of nonstandard bend geometries, including PCVN configurations with increased span, using on a micromechanics approach based on the Weibull stress model [26,23,27]. Given the current standardization scenario, in which non-standard fracture specimens are increasingly being utilized in routine fracture toughness testing, the present investigation, when taken together with previous studies, provides further motivation to develop fracture test standards incorporating non-standard fracture geometries.

Acknowledgments

This investigation is supported by Fundação de Amparo à Pesquisa do Estado de São Paulo (FAPESP) through research grant 2016/26024-1. The first author (VSB) would like to acknowledge the financial support from Coordenação de Aperfeiçoamento de Pessoal de Nível Superior (CAPES). The work of CR is also supported by the Brazilian Council for Scientific and Technological Development (CNPq) through grant 306193/2013-2. The authors acknowledge the many useful discussions and contributions of their colleagues Dr. S. Cravero (Tenaris Argentina – R&D Center) and Prof. Waldek W. Bose (University of São Paulo at São Carlos).

References

[1] American Welding Society. Welding handbook – volume 1: welding technology. 8th ed. AWS, 1987.
[2] International Organization for Standardization. Welding and allied processes – classification of geometric imperfections in metallic materials – Part 1: Fusion welding. ISO 6520-1:2007; 2007.
[3] Wallin K. Fracture toughness transition curve shape for ferritic structural steels. In: Teoh SHSH, Lee KH, editors. Joint FEFG/IICF international conference on fracture of engineering materials and structures , Singapore; 1991. p. 83–8.
[4] Wallin K. Irradiation damage effects on the fracture toughness transition curve shape for reactor pressure vessel steels. Int J Pres Ves Pip 1993;55:61–79.
[5] Wallin K. Master curve analysis of the Euro fracture toughness dataset. Eng Fract Mech 2002;69:451–81.
[6] McCabe DE, Merkle JG, Wallin K. An introduction to the development and use of the master curve method. ASTM manual series MNL 27. ASTM International; 2005.
[7] American Society for Testing and Materials. Standard test method for determination of reference temperature, T_0, for ferritic steels in the transition range. ASTM E1921-17a; 2017.
[8] Kirk M, Lott R, Kim C, Server W. Empirical validation of the master curve for irradiated and unirradiated reactor pressure vessel steels. In: American Society of Mechanical Engineers (ASME)/Japan Society of Mechanical Engineers (JSME) pressure vessels and piping conference , Honolulu, HI, USA; 1995.
[9] Joyce JA, Tregoning RL. Development of the T_0 reference temperature from precracked Charpy specimens. Eng Fract Mech 2001;68:861–94.
[10] Odette GR, Lucas GE. Embrittlement of nuclear reactor pressure vessels. J Mater 2001;53(7):18–22.
[11] U.S. Nuclear Regulatory Commission. Expanded materials degradation assessment (EMDA) – volume 3: aging of reactor pressure vessels, vol. 3. Tech rep. NUREG/CR-7153, USNRC; 2014.
[12] Nanstad R, Corwin W, Alexander D, Haggag F, Iskander S, McCabe D, et al. Heavy-section steel irradiation program on irradiation effects in light-water reactor pressure vessel materials. In: American Society of Mechanical Engineers (ASME)/Japan Society of Mechanical Engineers (JSME) pressure vessels and piping conference , Honolulu, HI, USA; 1995.
[13] Barbosa VS, Ruggieri C. Fracture toughness testing using non-standard bend specimens – Part I: Constraint effects and development of test procedure. Eng Fract Mech. doi: https://doi.org/10.1016/j.engfracmech.2018.03.028.
[14] American Society for Testing and Materials. Standard specification for high-strength low-alloy columbium-vanadium structural steel. ASTM A572; 2015.
[15] American Society for Testing and Materials. Standard test methods for tension testing of metallic materials. ASTM E8-16a; 2016.
[16] American Petroleum Institute. Fitness-for-service. API RP-579-1/ ASME FFS-1; 2007.
[17] American Society for Testing and Materials. Standard test method for notched bar impact testing of metallic materials. ASTM E23-16b; 2016.
[18] EricksonKirk MT, Shaikh A, EricksonKirk MA. Insights and observations arising from curve-fitting the Charpy V-notch and tensile data contained within the United States Light Water reactor surveillance database. ASME PVP 2008 pressure vessel and piping division conference. Chicago (IL): American Society of Mechanical Engineers; 2008.
[19] American Society for Testing and Materials. Standard test method for measurement of fracture toughness. ASTM E1820-17; 2017.
[20] Mann NR, Schafer RE, Singpurwalla ND. Methods for statistical analysis of reliability and life data. New York: Jonh Wiley & Sons; 1974.
[21] Anderson TL. Fracture mechanics: fundaments and applications. 3rd ed. Boca Raton (FL): CRC Press; 2005.

[22] Nevalainen M, Dodds RH. Numerical investigation of 3-D constraint effects on brittle fracture in SE(B) and C(T) specimens. Int J Fract 1995;74:131–61.
[23] Ruggieri C, Savioli RG, Dodds RH. An engineering methodology for constraint corrections of elastic-plastic fracture toughness – Part II:: Effects of specimen geometry and plastic strain on cleavage fracture predictions. Eng Fract Mech 2015;146:185–209.
[24] Mahgerefteh H, Denton G, Rykov Y. Pressurized CO_2 pipeline rupture. In: Hazard XX: IChemE symposium on process safety and environmental protection, symposium series 154. The Institution of Chemical Engineers; 2008.
[25] Cosham A, Eiber RJ. Fracture propagation of CO_2 pipelines. J Pipeline Eng 2008;7:115–24.
[26] Ruggieri C, Dodds RH. An engineering methodology for constraint corrections of elastic-plastic fracture toughness – Part I: A review on probabilistic models and exploration of plastic strain effects. Eng Fract Mech 2015;134:368–90.
[27] Ruggieri C. A probabilistic model including constraint and plastic strain effects for fracture toughness predictions in a pressure vessel steel. Int J Pres Ves Pip 2016;148:9–25.